



# Sensing of mercury ion using light induced aqueous leaf extract mediated green synthesized silver nanoparticles of *Cestrum nocturnum* L

Pradeep Kumar<sup>1</sup> · Piyush Kumar Sonkar<sup>2</sup> · Kavindra Nath Tiwari<sup>1</sup> · Amit Kumar Singh<sup>3</sup> · Sunil Kumar Mishra<sup>3</sup> · Jyoti Dixit<sup>1</sup> · Vellaichamy Ganesan<sup>4</sup> · Jasmeet Singh<sup>5</sup>

Received: 3 December 2021 / Accepted: 18 February 2022 / Published online: 23 February 2022  
© The Author(s), under exclusive licence to Springer-Verlag GmbH Germany, part of Springer Nature 2022

## Abstract

In this study, a simple, one-pot, and eco-friendly biosynthesis of silver nanoparticles (AgNPs) was accomplished with the use of aqueous leaves extract of *Cestrum nocturnum* L. (AECN). Different techniques like ultraviolet–visible (UV–Vis) spectrophotometry, Fourier transform infrared (FTIR), X-ray diffraction (XRD), transmission electron microscopy (TEM), and scanning area electron diffraction were used to investigate the optical, operational, and physical properties of the green synthesized AECN-AgNPs. The AECN-AgNPs were further used for the detection of Hg<sup>2+</sup> by UV–Vis and electrochemical methods. The disintegration of the AECN-AgNPs solution caused the formation of an Ag–Hg amalgam, which caused discoloration of the solution. Sensing performance for a variety of metals such as Na<sup>+</sup>, K<sup>+</sup>, Mg<sup>2+</sup>, Ca<sup>2+</sup>, Ni<sup>2+</sup>, Cu<sup>2+</sup>, Fe<sup>3+</sup>, Zn<sup>2+</sup>, Co<sup>2+</sup>, Cd<sup>2+</sup>, Pb<sup>2+</sup>, As<sup>3+</sup>, and Mn<sup>2+</sup> at 10-mM concentrations was measured in order to determine the selectivity of the sensor towards the Hg<sup>2+</sup>. For the electrochemical determination of 2 + Hg<sup>2+</sup>, AECN-AgNPs were immobilized on a glassy carbon (GC) electrode, and the resulting modified electrode (GC/AECN-AgNPs) was characterized by cyclic voltammetry. This phenomenon is advantageously used for the sensitive determination of trace level Hg<sup>2+</sup>. GC/AECN-AgNPs demonstrated a linear calibration range of 100 nM to 10 μM and a limit of detection of 21 nM for Hg<sup>2+</sup> determination.

**Keywords** *Cestrum nocturnum* · Hg<sup>2+</sup> sensor · Silver nanoparticles · Glassy carbon · Electrochemical · Cyclic voltammetry

Responsible Editor: Philippe Garrigues.

Piyush Kumar Sonkar, Kavindra Nath Tiwari, Sunil Kumar Mishra, and Vellaichamy Ganesan are equally contributed in this work.

✉ Kavindra Nath Tiwari  
kntiwari@bhu@gmail.com

- <sup>1</sup> Department of Botany, MMV, Banaras Hindu University, Varanasi 221005, India
- <sup>2</sup> Department of Chemistry, MMV, Banaras Hindu University, Varanasi 221005, India
- <sup>3</sup> Department of Pharmaceutical Engineering and Technology, Indian Institute of Technology, Banaras Hindu University, Varanasi 221005, India
- <sup>4</sup> Department of Chemistry, Institute of Science, Banaras Hindu University, Varanasi 221005, India
- <sup>5</sup> Department of Dravyaguna, Faculty of Ayurveda, Institute of Medical Sciences, Banaras Hindu University, Varanasi 221005, India

## Introduction

Mercuric ion (Hg<sup>2+</sup>) is considered the most stable toxic metal ion which pollutes the environment and affects human health (Toh et al. 2015; Tang et al. 2014; Zhou et al. 2013). Mercury is a heavy metal pollutant emitted by fossil fuel emissions (coal-burning thermal power plants), battery cells, mercury-based rituals, and hazardous material combustion (Park and Zheng 2012). It is reported that the Hg<sup>2+</sup> level in the human body is gradually increasing through the food chain, causing serious and permanent injuries to the nervous system and brain (Zheng et al. 2003; Wei et al. 2013; Agraz et al. 1995). Its toxicity affects human health and causes severe damage to the kidney, heart, and lungs, as well as reducing the immune system (Azevedo et al. 2012; Rice et al. 2014; Chang et al. 1992) of human beings. The development of a sensitive, simple, and reliable technique is required for the routine detection of Hg<sup>2+</sup> (Toh et al. 2015; Lou et al. 2011; Ding et al. 2016). Presently, a number of methods are available for Hg<sup>2+</sup> detection, which include

atomic absorption spectroscopy, atomic emission spectrometry, X-ray fluorescence spectrometry, colorimetric assay, and gas chromatography (Rey-Raap and Gallardo, 2012; Ioannidou et al. 2005; Aranda et al. 2013; Lin et al. 2016; Fang et al. 2016; Wu et al. 2012; Zaib et al. 2015). These techniques generally have high selectivity and sensitivity. However, sophisticated instruments, extensive sample pretreatments, and/or more samples are required, limiting their wide range of applications (Toh et al., 2015). Electrochemical methods are promising alternatives for sensitive  $\text{Hg}^{2+}$  determination in aqueous samples due to their low cost, high sensitivity, and short experimental time (Toh et al. 2015; Wei et al. 2013). The development of a well-organized method for the detection of  $\text{Hg}^{2+}$  is a matter of concern. Many different types of sensors have been developed, including those that use color, electrochemical methods, and fluorescence recognition (Cinti et al. 2016; Some et al. 2016; Wang and Bonakdar 1988). As a result, there is significant emphasis on the development of an effective sensor for the detection of mercury in the environment. For the determination of  $\text{Hg}^{2+}$  in the environment, several advanced instruments were used, including the inductively coupled plasma mass spectrometer (ICP-MS) (Cinti et al. 2016), the inductively coupled plasma optical emission spectrometer (ICP-OES) (Some et al. 2016), the cold vapor atomic absorption spectrometer (CVAAS) (Wang and Bonakdar, 1988), and the stripping voltammeter (Afkhami et al. 2012). The above instruments are expensive and time-consuming and necessarily involve a skilled operator for their handling. For the rapid detection of  $\text{Hg}^{2+}$ , a few technologies based on spectrophotometric and probes of specific metals have been developed (Cinti et al. 2016; Some et al. 2016; Wang and Bonakdar 1988; Afkhami et al. 2012; Suaarez et al. 2000).

Electrochemical methods have been tested for  $\text{Hg}^{2+}$  determination using various materials/electrodes such as graphene oxide-ionic liquid composites/gold nanoparticles (Zhou et al. 2013), silver nanoparticle modified glassy carbon electrode (Toh et al. 2015), screen-printed carbon (Cinti et al. 2016; Some et al. 2016), carbon paste (Wang and Bonakdar 1988; Afkhami et al. 2012), and titanium dioxide (Suaarez et al. 2000). In spite of the above methods and materials, a sensitive electrode/material is still required for cost-effective, selective, and real-time determination of trace-level  $\text{Hg}^{2+}$  at low over potentials. Nowadays, scientists are interested in developing  $\text{Hg}^{2+}$  detection techniques that are eco-friendly, involving biomolecules and natural materials. Medicinal plants contain several phytoconstituents which may be useful for this purpose.

*Cestrum nocturnum* L. belongs to the Solanaceae family. It is commonly known as a night blooming jasmine and is widely distributed all over tropical as well as subtropical areas of the world, including Australia, India, Southern China, and the USA. It is an important horticultural plant

used for ornamental and medicinal purposes. Several studies have demonstrated that it has a great deal of pharmacological activity, including antibacterial (Al-Reza et al. 2009), hepatoprotective activity (Qadir et al. 2014), and anticoagulant activity (Tyagi et al. 2016). It also contains biologically active phytochemicals like phenols, glycosides, saponins, and flavonoids.

The objective of the current work was to synthesize photo-induced green silver nanoparticles from aqueous leaf extract of *C. nocturnum* and to immobilize them in glassy carbon electrode for the detection of the  $\text{Hg}^{2+}$  ion.

## Materials and methods

### Chemicals and reagents

During the experiment, salts of various cations ( $\text{Pb}(\text{NO}_3)_2$ ,  $\text{KCl}$ ,  $\text{MgCl}_2$ ,  $\text{MnSO}_4$ ,  $\text{CaCl}_2$ ,  $\text{HgCl}_2$ ,  $\text{ZnCl}_2$ ,  $\text{CdCl}_2$ ,  $\text{CoCl}_2$ ,  $\text{NiCl}_2$ ,  $\text{CuCl}_2$ ,  $\text{As}_2\text{O}_3$ , and  $\text{FeCl}_3$ ) were used. Experimental salt solutions (1 mM) were made by mixing salt with Milli-q water and adjusting the pH with either 1.0 N HCl or 1.0 N NaOH. Before use, the glassware was immersed in chromic acid and rinsed thoroughly with double distilled water. All chemicals have been purchased from SRL Chemicals Pvt. Ltd., India. For the electrochemical experiments, triple distilled water was used.

### Instrumentation

The optical, operational, and physical properties of the green synthesized AECN-AgNPs were studied using UV–Visible, FTIR, X-ray diffraction (XRD), transmission electron microscopy (TEM), and scanning area electron diffraction (SAED). All the electrochemical measurements were carried out using CH instruments electrochemical workstation (CHI-660C, USA). A three-electrode system having glassy carbon (GC) or AECN-AgNPs immobilized GC (GC/AECN-AgNPs) as the working electrode, Ag/AgCl (saturated with KCl) as the reference electrode, and platinum wire as the counter electrode was used for electrochemical measurements.

### Preparation of leaf extract

Fresh leaves of *C. nocturnum* were taken from the campus of Banaras Hindu University, Varanasi, India, and washed repeatedly with double distilled water to remove dirt particles and other adhering contaminants before being used to make the aqueous leaf extract. Thereafter, the leaves were allowed to air dry in the shade to completely remove moisture. The dried leaves were then grinded, and 25 g of leaf powder was added to 100 ml of double distilled water and

boiled for 5 min at 60 °C. *Aqueous filtrate of C. nocturnum* was obtained by using Whatman filter paper No. 1. The prepared AECN was kept at 4 °C as a stock solution for future use.

### Biosynthesis of AECN-AgNPs

For biosynthesis of AECN-AgNPs, 2 ml of AECN extract (1%) was added to 100 mL of AgNO<sub>3</sub> (1 mM) solution. The reaction mixture was exposed to bright sunlight for 30 min. The reaction mixture had a neutral pH. In bright sunlight, the ambient temperature was 38 °C, with a solar intensity of 536 lx. The confirmation of synthesis of AECN-AgNPs was measured by using a UV–Vis spectrophotometer (Simadazu1800, Japan) between the ranges of 250 and 700 nm. All AECN-AgNPs biosynthesis procedures were carried out in direct sunlight in order to optimize the other factors individually. Factors like AECN inoculum dose (0.25% to 4.0%), duration of sunlight exposure (1–30 min), and AgNO<sub>3</sub> concentration (0.5 to 5 mM) were optimized for proper synthesis of AECN-AgNPs. The biosynthesized AECN-AgNPs were isolated by centrifugation at 15,000 rpm for 15 min after the reaction was completed at these optimized reaction conditions. Further, AECN-AgNPs were re-dispersed in Milli-Q water to remove the organic substances and natural compounds. The procedure was executed multiple times, and the desired amount of AECN-AgNPs was obtained by drying.

### Preparation of GC/AECN-AgNPs electrode

The GC electrode was cleaned to a mirror finish by hand polishing on a cloth pad with an aqueous neutral alumina slurry and then ultra-sonicated in water. The AECN-AgNPs suspension (10 µL, 1.0 mM) was drop casted on a dry and clean GC electrode and dried for 2 h. The resulting electrode, abbreviated as GC/AECN-AgNPs, was used for electrochemical studies and for the electrochemical determination of Hg<sup>2+</sup>.

### Sensing of multi metal ion

The AECN-AgNPs solution was being used as a key solution for various metal ion detection. A fixed concentration (200 µL) of various metal ion solutions (Na<sup>+</sup>, K<sup>+</sup>, Mn<sup>2+</sup>, Mg<sup>2+</sup>, Ca<sup>2+</sup>, Ni<sup>2+</sup>, Cu<sup>2+</sup>, Zn<sup>2+</sup>, Fe<sup>3+</sup>, Co<sup>2+</sup>, As<sup>3+</sup>, Cd<sup>2+</sup>, Pb<sup>2+</sup>, and Hg<sup>2+</sup>) was added to an AECN-AgNPs (5 ml) solution, and the absorption spectra was recorded using a UV–Vis spectrophotometer. The highest sensing ability of AECN-AgNPs and the decolorization of AECN-AgNPs solution were measured in the presence of Hg<sup>2+</sup>. Therefore, various concentrations (10 nM to 100 µM) of Hg<sup>2+</sup> were applied for the determination of the linear sensing range by using AECN-AgNPs solution.

### Effect of pH on the detection of Hg<sup>2+</sup>

To evaluate the Hg<sup>2+</sup> detecting ability of AECN-AgNPs at different pH (4–10), the 100 µM of HgCl<sub>2</sub> was spiked in double distilled water. After that, the pH of the HgCl<sub>2</sub> solution was maintained from pH 4 to pH 10 through NaOH (1 N) and HCl (1 N). When 1 ml of HgCl<sub>2</sub> solution of each pH was added to 1 ml dark brown solution of AECN-AgNPs, a distinct color change of the solution was observed. The spectra were recorded by the UV–Vis spectrophotometer at different time intervals (0 to 10 min).

### Characterization of synthesized AECN-AgNPs

TEM (TECNAI 20 G2) performed at a voltage of 100–200 kV was used for the analysis of the shape and size of the synthesized AgNPs. A thin film of green synthesized AECN-AgNPs sample was prepared by dropping a small amount on copper grid, and extra sample was removed by using blotting paper and kept it for drying at room temperature for 15–30 min. FTIR for the AECN-AgNPs powder and extract of the *C. nocturnum* was used to identify the functional groups in a (Bruker) spectrophotometer IR affinity-1 by employing the KBr pellet technique and registering amplitude waves ranging from 400 to 4000 cm<sup>-1</sup>. The crystallinity of the biosynthesized AECN-AgNPs was demonstrated by X-ray diffraction (Rigaku Miniflex II). The circular scattering rings observed in the selected area electron diffraction represent the crystalline nature of the biosynthesized AgNPs.

### Colorimetric detection of Hg<sup>2+</sup> in real water samples

For the sensing of Hg<sup>2+</sup> ions in real water samples, the water samples such as drinking water, tap water, and river water were collected and filtered via the Whatman filter paper. These water samples were treated with 200 µl of three different concentrations of Hg<sup>2+</sup> (50, 100, and 200 nM), and the colorimetric changes in the presence of AECN-AgNPs (200 µl) solution were examined using a UV–Vis spectrophotometer.

### Statistical analysis

All of the tests have been done three times. The data collected throughout the study was analyzed and represented as mean ± SD.

## Results and discussion

### Photo-induced biosynthesis of AECN-AgNPs

AECN (yellow color) was mixed with  $\text{AgNO}_3$  solution (colorless) and kept for 30 min under direct sunlight. The color of the reaction mixture changed from yellow to brown color (Fig. 1); this change in color indicates the biosynthesis of AECN-AgNPs. UV–Vis spectrophotometer result showed a sharp band in between 400 and 500 nm, while alone, AECN and  $\text{AgNO}_3$  solution did not show any SPR band (Fig. 1). The sharp SPR band indicates the biosynthesis of the AECN-AgNPs. The above result emphasizes the importance of sunlight in AECN-AgNPs biosynthesis. In order to maximize the efficiency of AECN-AgNPs biosynthesis, different factors like duration of light exposure, inoculum concentration, silver nitrate concentration, and pH of reaction mixtures were optimized.

### Effect of light exposure on biosynthesis of AECN-AgNPs

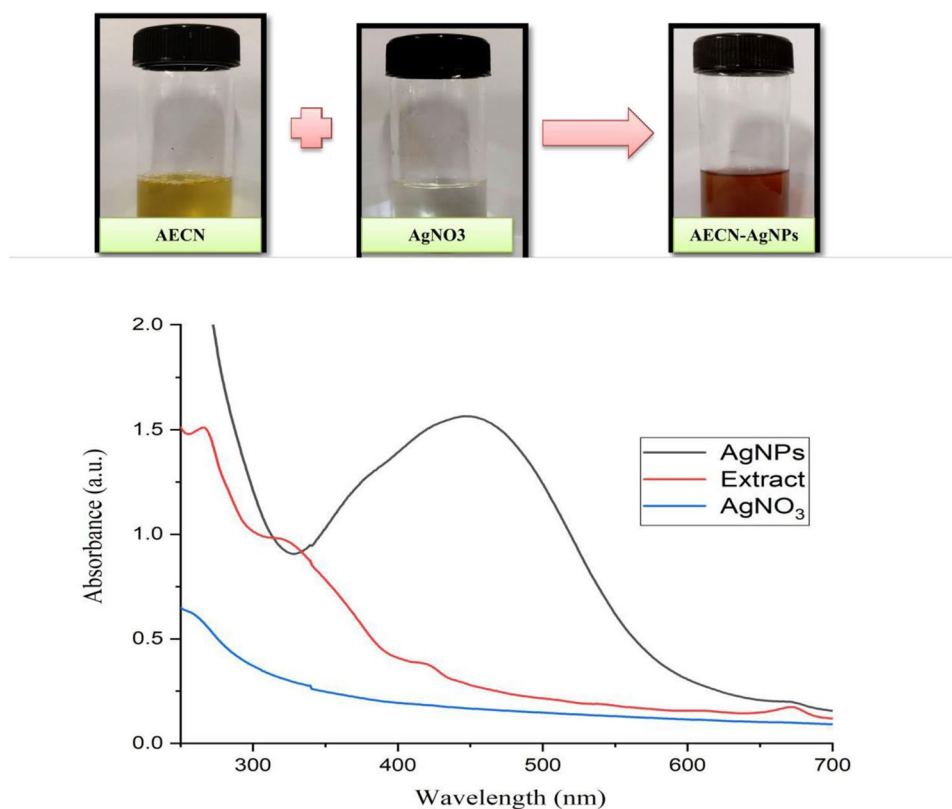
The control samples containing  $\text{AgNO}_3$  or AECN alone did not show any change in color. Thus, the biosynthesis of AECN-AgNPs requires both  $\text{AgNO}_3$  and AECN. In the previous report (Kumar et al. 2017), the presence of light in the biosynthesis of AgNPs was required. The experiments were

performed to optimize the duration of light exposure for the biosynthesis of AECN-AgNPs by exposing the reaction mixture to direct sunlight for various periods of time (1–30 min). It was observed that when reaction mixtures were subjected to direct sunlight, they changed color instantly within just a few seconds. UV spectra of the reaction mixture after each time period were recorded. Results revealed that SPR band intensity was increased with an increased duration of light exposure (Kumar et al. 2016a, b). At 30 min of sunlight exposure, the SPR band was very sharp. Furthermore, there was no change in SPR intensity (Fig. S1). It confirmed that the 30-min sunlight exposures to the reaction mixture were sufficient for AECN-AgNPs biosynthesis.

### Effect of inoculum (AECN) dose on biosynthesis of AECN-AgNPs

To optimize the suitable concentration of the inoculums for efficient biosynthesis of nanoparticles, different concentrations (0.25% to 4%) of AECN were added to the reaction mixture, while other factors were kept constant. After 30 min of exposure to direct sunlight, the color of the reaction mixture changed from yellow to brown (Fig. S2) (Kumar et al. 2016a, b). Results revealed that 0.25% and 0.5% of AECN inoculum doses in the reaction mixtures produced a single, broader, and less intense SPR band. This

**Fig. 1** UV–Vis spectra of bio-synthesized AECN-AgNPs



confirmed that there was no proper synthesis of  $\text{AgNO}_3$ . Further, on increasing the AECN inoculum dose from 1.0 to 4.0%, the intensity and clarity of the SPR band enhanced after 30 min of light exposure, indicating good biosynthesis of AECN-AgNPs in higher proportions (Fig. S2). UV spectra of the reaction mixture supplemented with 4.0% AECN inoculum showed maximum absorbance at 452 nm. Thus, AECN-AgNPs synthesis was optimized at 4.0% AECN inoculum (Kumar et al. 2017). AECN-AgNPs were also synthesized at high AECN dosages, but clumping of AECN-AgNPs takes place. The sharpening and expansion of the SPR band occurred due to the clump formation of AECN-AgNPs (Kumar et al. 2016a, b).

### Effect of $\text{AgNO}_3$ concentration on biosynthesis of AECN-AgNPs

To decide the most effective concentration of  $\text{AgNO}_3$  for the biosynthesis of AECN-AgNPs, different  $\text{AgNO}_3$  concentrations (0.5 mM to 5 mM) were added to the reaction mixture supplemented with 4% AECN and exposed to sunlight for 30 min. The SPR bands of AECN-AgNPs with various  $\text{AgNO}_3$  concentrations (0.5 mM, 1.0 mM, 2.0 mM, 3.0 mM, 4.0 mM, 5.0 mM) are shown in Figure S3. Based on the above findings, the color of the reaction mixture darkened progressively as the concentration of  $\text{AgNO}_3$  (Kumar et al. 2016a, b) was increased after 30 min direct sunlight exposure (Fig. S3). As a result, 5 mM  $\text{AgNO}_3$  was best for AECN-AgNPs biosynthesis.

### Effect of pH of reaction mixture

The pH is another important parameter that influences the biosynthesis of silver nanoparticles. The pH of the reaction mixture also affects the size as well as the shape of biosynthesized AgNPs. It has the ability to alter the charges of bio molecules, which might be affecting its stabilizing and capping properties. The peak absorption wavelength shifts from 427 to 439 nm as the pH increases from 4 to 10 (Fig. S4). The above results indicate that pH 6 is the most suitable for the synthesis of AECN-AgNPs. It was observed that when AECN was added to different pH solutions, the color of the reaction mixture changed very fast from yellow to dark brown color with increasing pH. Peak shifting at various pH levels suggests about size as well as shape of the green silver nanoparticles, which was regulated by the pH of the reaction mixture (Kumar et al. 2016a, b).

## Characterization of biosynthesized AECN-AgNPs

### HRTEM analysis

The shape, size, and structure of silver nanoparticles were investigated by using the HRTEM technique (Kumar

et al. 2016a, b). HRTEM images of the AECN-AgNPs (Fig. 2A–B) clearly indicate that synthesized nanoparticles are highly stable and are spherical in shape with a smooth surface without agglomeration. The particle size distribution of AECN-AgNPs was observed between 2 and 20 nm with an average particle size of 10 nm (Fig. 2C). HR TEM images of selected area electron diffraction patterns (SAED) of AECN-AgNPs confirmed the crystalline characteristics of the silver nanoparticle (Fig. 2D).

### XRD

The diffraction peaks were visible in the XRD pattern of biosynthesized AECN-AgNPs at  $32.17^\circ$ ,  $44.47^\circ$ ,  $64.34^\circ$ , and  $76.99^\circ$  which were related to Bragg reflections (111), (200), (220), and (311) respectively (JCPDS file no. 00–004–0783). The crystalline planes of metallic silver's face-centered cubic (fcc) crystal structure are represented by these Bragg reflections (Fig. 3).

### FTIR spectral analysis

FTIR analysis of AECN showed peaks at 3361, 3017, 2930, 1635, 1541, 1428, 1292, 1078, 868, 842.9, and  $790.8\text{ cm}^{-1}$ . Peaks 1382, 1246, 1075, 839.1, 824.8, and  $777.3\text{ cm}^{-1}$  were found in the AECN-AgNPs (Fig. S4). The -OH and C-H groups were reduced and sifted at  $3356\text{ cm}^{-1}$  and  $3011\text{ cm}^{-1}$  in the FTIR spectra of AECN-AgNPs. The peak shifting and intensity reduction represent the extract's -OH and C-H groups involved in AgNPs formation. Methylene C-H stretch, alkenyl C=C stretch, aliphatic nitro compound, and organic sulphate groups were also involved in AECN-AgNPs formation. FTIR spectra of AECN-AgNPs showed weaker peaks than AECN. As shown above in Figure S5, AECN-AgNPs lacked all the AECN peaks. It means that the carboxyl, hydroxyl, peroxide, nitro, and organic sulfate groups found in AECN phytochemicals play a role in silver nanoparticle reduction and stabilization (Coates 2006).

### AECN-AgNPs-based detection of $\text{Hg}^{2+}$

The biosynthesized AECN-AgNPs were evaluated as spectrophotometric sensor for  $\text{Hg}^{2+}$  recognition under optimum conditions. The potential of AECN-AgNPs to detect metal ions was investigated separately for  $\text{Na}^+$ ,  $\text{K}^+$ ,  $\text{Mg}^{2+}$ ,  $\text{Ca}^{2+}$ ,  $\text{Ni}^{2+}$ ,  $\text{Cu}^{2+}$ ,  $\text{Fe}^{3+}$ ,  $\text{Zn}^{2+}$ ,  $\text{Co}^{2+}$ ,  $\text{Cd}^{2+}$ ,  $\text{Pb}^{2+}$ ,  $\text{As}^{3+}$ ,  $\text{Mn}^{2+}$ , and  $\text{Hg}^{2+}$  at a fixed volume of 200  $\mu\text{l}$  of metal ion solution mixed with 5 ml of AECN-AgNPs solution. The intensity of the SPR band changed slightly when different metals ( $\text{Na}^+$ ,  $\text{K}^+$ ,  $\text{Mg}^{2+}$ ,  $\text{Ca}^{2+}$ ,  $\text{Ni}^{2+}$ ,  $\text{Cu}^{2+}$ ,  $\text{Fe}^{3+}$ ,  $\text{Zn}^{2+}$ ,  $\text{Co}^{2+}$ ,  $\text{Cd}^{2+}$ ,  $\text{Pb}^{2+}$ ,  $\text{As}^{3+}$ ,  $\text{Mn}^{2+}$ , and  $\text{Hg}^{2+}$ ) were added to the AECN-AgNPs solution, whereas the color of the solution stayed unchanged (Fig S6A). While  $\text{Hg}^{2+}$



**Fig. 2** HRTEM images of AECN-AgNPs (**A–B**), histogram showing particles size distribution of AECN-AgNPs (**C**), and SAED pattern of crystalline AECN-AgNPs (**D**)

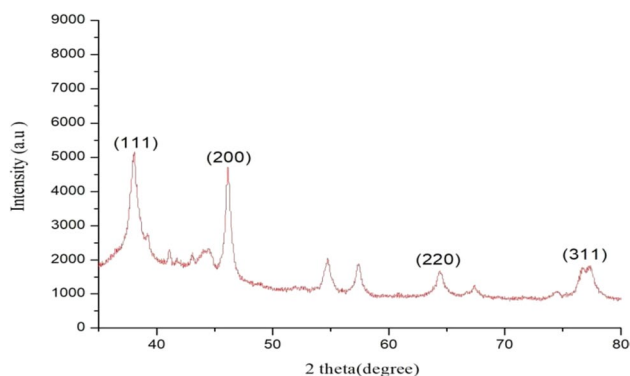
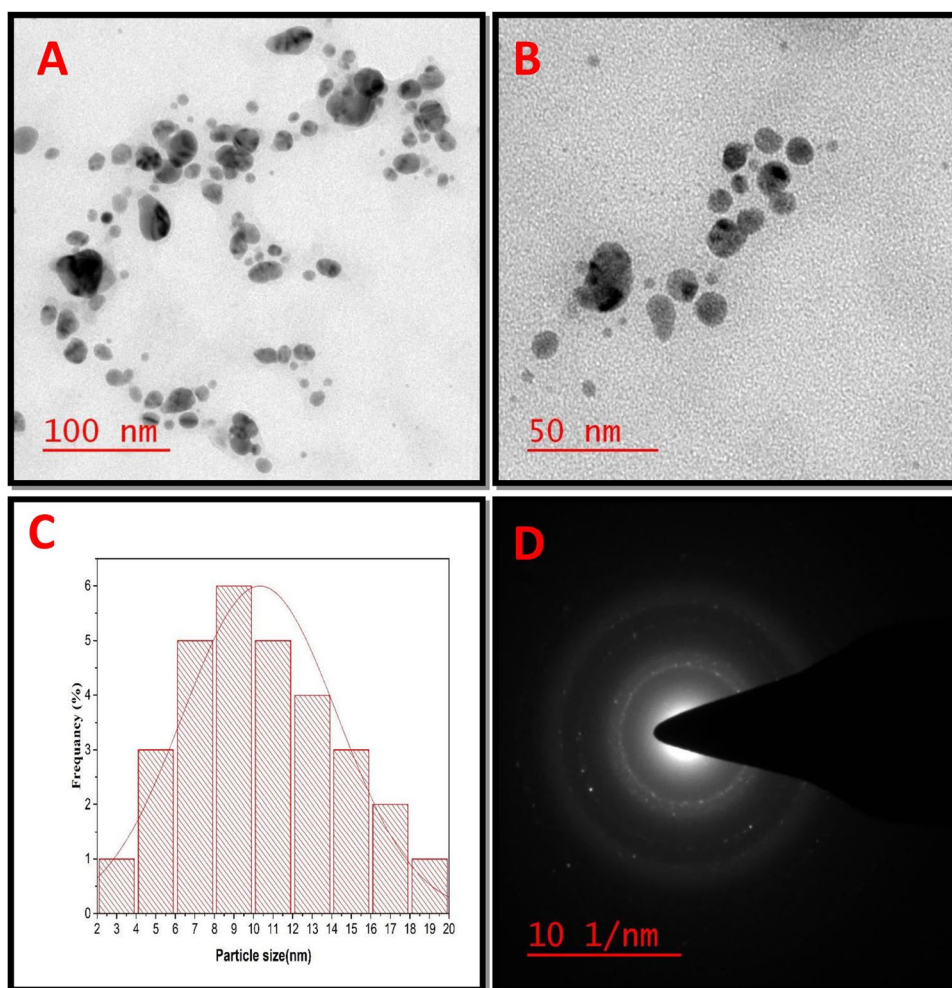


**Fig. 3** XRD pattern of AECN-AgNPs

has been added, however, the intensity of the SPR band shifted significantly, and the color of the solution changed from brown to colorless. Based on calorimetry data, it was clear that  $\text{Hg}^{2+}$  shows the highest sensitivity factor as compared to other metals (Fig. S6B). It has been shown that AECN-AgNPs can identify  $\text{Hg}^{2+}$  with high sensitivity and

specificity (Kumar et al. 2017; Chen et al. 2013). Adding  $\text{Hg}^{2+}$  metal ions to the AECN-AgNPs solution revealed that the absorbance intensity changed as the concentration of  $\text{Hg}^{+}$  increased (Fig. S7A). Figure S7B shows the linear relationship between the change in absorption spectra and different concentrations of  $\text{Hg}^{2+}$ .

#### Effect of pH on the detection of $\text{Hg}^{2+}$

AECN-AgNPs detect  $\text{Hg}^{2+}$  metal ions in a wide range of diverse physiological pH of water systems. Because of the high stability of AECN-AgNPs over a wide pH range, we were able to investigate its  $\text{Hg}^{2+}$  sensing capability at various pH levels. AECN-AgNPs show different sensing efficacy for pH 4 to pH 10 (Fig. S8–14), but high sensing of  $\text{Hg}^{2+}$  ions took place at pH 6 ( $\lambda$  max 248 nm) at 1 min (Fig. S10), while pH 4, 5, 7, 8, 9, and 10 also detect  $\text{Hg}^{2+}$  but take more time in comparison to pH 6. Based on our findings, it is clear that at pH 6, high sensing of  $\text{Hg}^{2+}$  ions took place (Fig. S10 & Table S1).

### Electrochemical characterization of the modified electrode

Cyclic voltammetry (CV) response of the GC/AECN-AgNPs electrode was recorded in 0.1 M KCl solution at a scan rate of 20 mVs<sup>-1</sup> (Fig. 4A). GC/AECN-AgNPs shows oxidation and reduction signals at +0.12 and -0.54 V, respectively, which may be attributed to the oxidation of Ag<sup>0</sup> to Ag<sup>+</sup> and the reduction of Ag<sup>+</sup> to Ag<sup>0</sup>, respectively (Goulart et al. 2018; Sonkar and Ganesan 2015; Sonkar et al. 2016; Tang et al. 2009; Bard and Faulkner, 1980). To get a stable oxidation peak, the GC/AECN-AgNPs electrode was initially subjected to 10 continuous CV scans, and after getting a constant oxidation response, the electrode was used for further electrochemical experiments. The CV response of GC/AECN-AgNPs was recorded with different scan rates (10 to 200 mVs<sup>-1</sup>) and is shown in Fig. 4B. On increasing the scan rate, the peak current was also increased linearly (inset of Fig. 4B). It indicates a surface confined process as expected for the AECN-AgNPs immobilized electrodes (Toh et al. 2015; Bard and Faulkner 1980).

### Electrochemical determination of Hg<sup>2+</sup> ions

In the absence of Hg<sup>2+</sup> ions, the linear sweep voltammetry (LSV) of GC electrode (Fig. 5A-a) does not exhibit any significant redox signals. However, GC/AECN-AgNPs (Fig. 5A-b) represents an oxidation signal due to the oxidation of AgNPs at 1.10 V in the absence of Hg<sup>2+</sup> ions (vide supra). In the presence of Hg<sup>2+</sup> ions, GC/AECN-AgNPs (Fig. 5A-c) displays high oxidation peak current (36.1 μA) at 0.18 V. This current response is much higher than that

observed at bare GC electrode (0.17 V, 8.1 μA) under similar conditions (Fig. 5A-d).

It is known that the Hg<sup>2+</sup> ions in the presence of an excess of Cl<sup>-</sup> ions undergo to form HgCl<sub>4</sub><sup>2-</sup> which is further converted to Hg<sub>2</sub>Cl<sub>2</sub> (Wei et al. 2013). Accordingly, the oxidation signal observed at the GC/AECN-AgNPs electrode in the presence of Hg<sup>2+</sup> may be due to the oxidation of Hg<sup>+</sup> to Hg<sup>2+</sup> ions (Wei et al. 2013). This indicates that the Hg<sup>+</sup> is electro catalytically oxidized to form Hg<sup>2+</sup> at the GC/AECN-AgNPs electrode and this phenomenon can be used for the sensitive determination of Hg<sup>2+</sup> originally present in a sample. The LSV oxidation peak current continuously increases with an increase in the concentration of added Hg<sup>2+</sup> (Fig. 5B). The oxidation current reaches to a saturation level at high concentrations (> 20 μM) of Hg<sup>2+</sup> probably due to the saturation of AECN-AgNPs catalytic sites (Tang et al. 2009; Bard and Faulkner, 1980) (Fig. 5C). The linear calibration range for the determination of Hg<sup>2+</sup> at the GC/AECN-AgNPs electrode is found to be 100 nM to 10 μM (Fig. 5D). The limit of detection (3σ/m, where σ = standard deviation, m = slope of the calibration plot) is found to be 21 nM. These studies demonstrate the trace level determination of Hg<sup>2+</sup> using the prepared AECN-AgNPs. In the electrochemical experiment, Hg<sup>2+</sup> was determined using AgNPs. The following section discusses a proposed mechanism for the electrochemical determination of Hg<sup>2+</sup> at the AgNPs modified electrode (Bhattacharjee and Chakraborty 2014; Suherman et al. 2017; Rastogi et al. 2014). The proposed reaction between Hg<sup>2+</sup> and AgNPs may occur in the following steps:

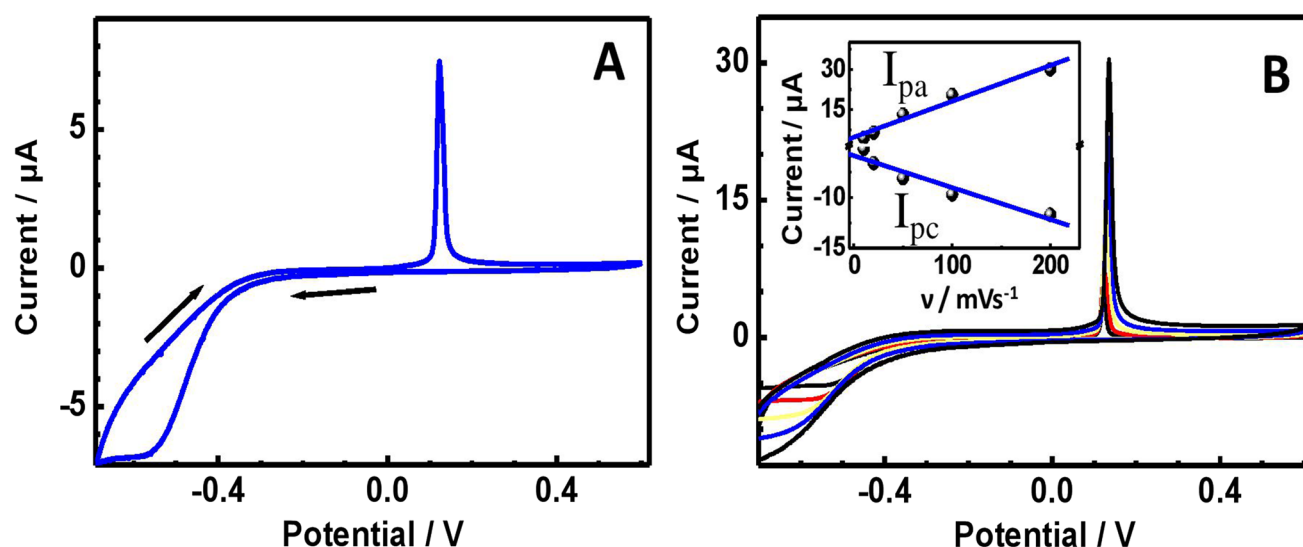


**Fig. 4** CV response of GC/AECN-AgNPs at a scan rate of 20 mVs<sup>-1</sup> in 0.1 M KCl (A), CV response of GC/AECN-AgNPs with different scan rates (10, 20, 50, 100, and 200 mVs<sup>-1</sup>) in 0.1 M KCl. Inset represents the plot between peak currents and scan rates (B)

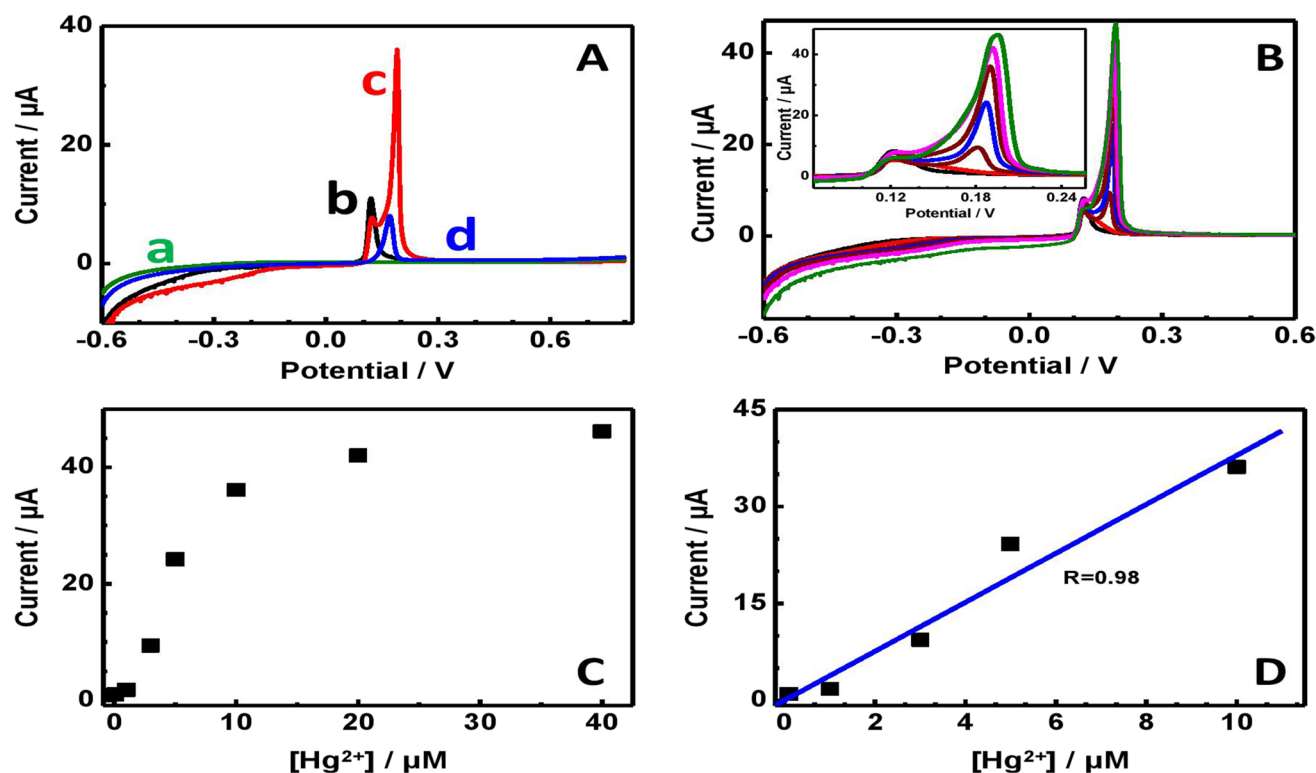
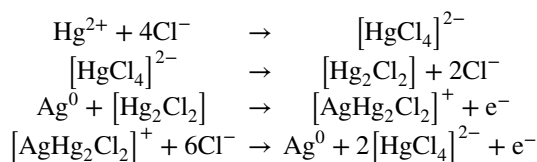


**Fig. 5** **A** LSV response of GC (a, d) and GC/AECN-AgNPs (b, c) in absence (a, b) and presence (c, d) of 10  $\mu\text{M}$   $\text{Hg}^{2+}$  in 0.1 M KCl at a scan rate of 20  $\text{mVs}^{-1}$ . **B** LSV response at GC/AECN-AgNPs with different additions of  $\text{Hg}^{2+}$  from 100 nM to 40  $\mu\text{M}$ . Inset represents

the zoomed view of the oxidation signals. **C** Plot representing the variation of oxidation current for  $\text{Hg}^{2+}$  with respect to its concentration. **D** Calibration plot for  $\text{Hg}^{2+}$  determination from 100 nM to 10  $\mu\text{M}$



## Practical application

The proposed sensing activity for the detection of  $\text{Hg}^{2+}$  at a nanomolar level may be applied to different samples. Here, it has been utilized in the detection of the  $\text{Hg}^{2+}$  level of four water samples (drinking water, tap water, pond water, and river water). A blank test was performed by the addition of a certain volume of water sample spiked with NaCl aqueous solution, and no change in spectra was found. A recovery experiment using different concentrations of  $\text{Hg}^{2+}$ , including the maximum permitted level (200 nM), was also performed. A good recovery (more than 96%) and RSD (relative standard deviation) less than 5% were obtained as shown in Table S2.

The final outcome reveals that the composition of the drinking water and tap does not significantly interfere with  $\text{Hg}^+$  detection in comparison of the pond and river water

sample. There may be a potential application of our proposed spectrophotometric method for the detection of  $\text{Hg}^+$  toxicity in real water samples.

## Conclusions

The AECN-AgNPs were successfully synthesized via a green method using *C. nocturnum* aqueous leaf extract. The synthesized AECN-AgNPs were characterized by UV–Vis spectroscopy, TEM, XRD, and FTIR. The average particle size of AECN-AgNPs was 10 nm, and the shape of the nanoparticles was spherical. The biosynthesized AECN-AgNPs also showed the ability to specifically sense harmful  $\text{Hg}^{2+}$  ions in a wide pH range at different time intervals. AECN-AgNPs were immobilized on the GC electrode, and the modified electrode, GC/AECN-AgNPs, demonstrates high electro catalytic activity for the oxidation of  $\text{Hg}^+$  which can be used for the determination of  $\text{Hg}^{2+}$  originally present in a sample. The linear calibration range and detection limits are 100 nM to 10  $\mu\text{M}$  and 21 nM, respectively. The proposed electrode, GC/AECN-AgNPs, could be a promising electrochemical sensor for the determination of trace level of  $\text{Hg}^{2+}$  in biological, pharmaceutical, food, and water samples.



The proposed colorimetric assay holds great potential for the safety control of drinking water and the determination of  $\text{Hg}^{2+}$  concentrations in various other water samples. Conclusively, AECN-AgNPs is an effective material for the detection of  $\text{Hg}^{2+}$  using electrochemical and absorption methods.

**Supplementary Information** The online version contains supplementary material available at <https://doi.org/10.1007/s11356-022-19357-x>.

**Author contribution** P Kumar: optimization of AECN-AgNPs synthesis. KN Tiwari, SK Mishra: supervision, methodology. PK Sonkar and V Ganesan: electrochemical detection and validation of  $\text{Hg}^{2+}$  sensing. AK Singh, J Singh, JDixit: plant material collection and extract preparation.

**Funding** This paper was supported in part from grant from UGC (F-1–17-1/2014–15/RGNF-2014–15-SC-UTT-58260) to New Delhi, Government of India, and is gratefully acknowledged. PKS acknowledges the University Grant Commission, New Delhi, India (UGC No.F.30–431/2018 (BSR), M-14–58), and Institute of Eminence (IoE) Seed Grant, Banaras Hindu University, India (Scheme No.6031), for the financial support. Author Kavindra Nath Tiwari also acknowledges to IoE, Banaras Hindu University, Varanasi, India, for the financial support for the research work (Scheme No.6031).

**Data availability** Data used in this study are freely available to the public from the described sources in the method section.

## Declarations

**Ethics approval and consent to participate** Not applicable.

**Consent for publication** Not applicable.

**Competing interests** The authors declare no competing interests.

## References

- Afkhami A, Madrakian T, Sabounchei SJ, Rezaei M, Samiee S, Pourshahbaz M (2012) Construction of a modified carbon paste electrode for the highly selective simultaneous electrochemical determination of trace amounts of mercury(II) and cadmium(II). *Sens Actuators B Chem*. <https://doi.org/10.1016/j.snb.2011.10.073>
- Agraz R, Sevilla MT, Hernandez L (1995) Voltammetric quantification and speciation of mercury compounds. *J Electroanal Chem*. [https://doi.org/10.1016/0022-0728\(95\)03955-G](https://doi.org/10.1016/0022-0728(95)03955-G)
- Al-Reza SM, Rahman A, Kang SC (2009) Chemical composition and inhibitory effect of essential oil and organic extracts of *Cestrum nocturnum* L. on food-borne pathogens. *Int J Food Sci Technol*. <https://doi.org/10.1111/j.1365-2621.2009.01939.x>
- Aranda PR, Colombo L, Perino E, de Vito IE, Raba J (2013) Solid-phase preconcentration and determination of mercury(II) using activated carbon in drinking water by X-ray fluorescence spectrometry. *X-Ray Spectrom*. <https://doi.org/10.1002/xrs.2440>
- Azevedo BF, Furieri LB, Peçanha FMI, Wiggers GA et al (2012) Toxic effects of mercury on the cardiovascular and central nervous systems. *J Biomed Biotechnol*. <https://doi.org/10.1155/2012/949048>
- Bard AJ, Faulkner LR (1980) *Electrochemical methods fundamentals and applications*, 2nd edn. Wiley, New York. <https://doi.org/10.1021/ed060pa25>
- Bhattacharjee Y, Chakraborty A (2014) Label-free cysteamine-capped silver nanoparticle-based colorimetric assay for Hg (II) detection in water with subnanomolar exactitude. *ACS Sustain Chem Eng*. <https://doi.org/10.1021/sc500339n>
- Chang LW (1992) The concept of direct and indirect neurotoxicity and the concept of toxic metal/essential element interactions as a common biomechanism underlying metal toxicity. In: Isaacson RL, Jensen KF (eds) *The vulnerable brain and environmental risks*. Springer, Boston, pp 61–82. <https://doi.org/10.1021/ac00153a011>
- Chen L, Fu X, Lu W, Chen L (2013) Highly sensitive and selective colorimetric sensing of  $\text{Hg}^{2+}$  based on the morphology transition of silver nanoprisms. *ACS Appl Mater Interfaces*. <https://doi.org/10.1021/am3020857>
- Cinti S, Santella F, Moscone D, Arduini F (2016)  $\text{Hg}^{2+}$  detection using a disposable and miniaturized screen-printed electrode modified with nanocomposite carbon black and gold nanoparticles. *Environ Sci Pollut Res*. <https://doi.org/10.1007/s11356-016-6118-2>
- Coates J (2006) Interpretation of infrared spectra a practical approach. In: Meyers RA (ed) *Encyclopedia of analytical chemistry*. Wiley, Chichester. <https://doi.org/10.1002/9780470027318.a5606>
- Ding Y, Wang S, Li J, Chen L (2016) Nanomaterial-based optical sensors for mercury ions. *Trends Anal Chem*. <https://doi.org/10.1016/j.trac.2016.05.015>
- Fang Y, Pan Y, Li P, Xue M, Pei F, Yang W, Ma N, Hu Q (2016) Simultaneous determination of arsenic and mercury species in rice by ion-pairing reversed phase chromatography with inductively coupled plasma mass spectrometry. *Food Chem*. <https://doi.org/10.1016/j.foodchem.2016.07.003>
- Goulart LA, Gonçalves R, Correa AA, Pereira EC, Mascaro LH (2018) Synergic effect of silver nanoparticles and carbon nanotubes on the simultaneous voltammetric determination of hydroquinone, catechol, bisphenol A and phenol. *Microchim Acta*. <https://doi.org/10.1007/s00604-017-2540-5>
- Ioannidou MD, Zachariadis GA, Anthemidis AN, Stratis JA (2005) Direct determination of toxic trace metals in honey and sugars using inductively coupled plasma atomic emission spectrometry. *Talanta*. <https://doi.org/10.1016/j.talanta.2004.05.018>
- Kumar V, Bano D, Mohan S, Singh DK, Hasan SH (2016a) Sunlight-induced green synthesis of silver nanoparticles using aqueous leaf extract of *Polyalthia longifolia* and its antioxidant activity. *Mater Lett*. <https://doi.org/10.1016/j.matlet.2016.05.097>
- Kumar V, Singh DK, Mohan S, Hasan SH (2016b) Photo-induced biosynthesis of silver nanoparticles using aqueous extract of *Erigeron bonariensis* and its catalytic activity against Acridine Orange. *J Photochem Photobiol B Biol*. <https://doi.org/10.1016/j.jphotobiol.2015.12.011>
- Kumar V, Singh DK, Mohan S, Bano D, Gundampati RK, Hasan SH (2017) Green synthesis of silver nanoparticle for the selective and sensitive colorimetric detection of mercury (II) ion. *J Photochem Photobiol B Biol*. <https://doi.org/10.1016/J.JPHOTOBIOL.2017.01.022>
- Lin Y, Yang Y, Li Y, Yang L, Hou X, Feng X, Zheng C (2016) Ultrasensitive speciation analysis of mercury in rice by headspace solid phase microextraction using porous carbons and gas chromatography-dielectric barrier discharge optical emission spectrometry. *Environ Sci Technol*. <https://doi.org/10.1021/acs.est.5b04328>
- Lou T, Chen Z, Wang Y, Chen L (2011) Blue-to-red colorimetric sensing strategy for  $\text{Hg}^{2+}$  and  $\text{Ag}^{+}$  via redox-regulated surface chemistry of gold nanoparticles. *ACS Appl Mater*. <https://doi.org/10.1021/am200130e>
- Park JD, Zheng W (2012) Human exposure and health effects of inorganic and elemental mercury. *J Prev Med Public Health*. <https://doi.org/10.3961/jpmph.2012.45.6.344>
- Qadir MI, al Murad MS, Ali M, Saleem M, Farooqi AA (2014) Hepatoprotective effect of leaves of aqueous ethanol extract of *Cestrum*

- nocturnum* against paracetamol-induced hepatotoxicity. Bangladesh J Pharmacol. <https://doi.org/10.3329/bjp.v9i2.17770>
- Rastogi PK, Ganesan V, Krishnamoorthi S (2014) A promising electrochemical sensing platform based on a silvernanoparticles decorated copolymer for sensitive nitrite determination. J Mater Chem A. <https://doi.org/10.1039/C3TA13794E>
- Rey-Raap N, Gallardo A (2012) Determination of mercury distribution inside spent compact fluorescent lamps by atomic absorption spectrometry. Waste Manage. <https://doi.org/10.1016/j.wasman.2011.12.001>
- Rice KM, Walker EM, Wu M, Gillette C, Blough ER (2014) Environmental mercury and its toxic effects. J Prev Med Public Health. <https://doi.org/10.3961/jpmph.2014.47.2.74>
- Some IT, Sakira AK, Mertens D, Ronkart SN, Kauffmann JM (2016) Determination of groundwater mercury (II) content using a disposable gold modified screen printed carbon electrode. Talanta. <https://doi.org/10.1016/j.talanta.2016.02.033>
- Sonkar PK, Ganesan V (2015) Synthesis and characterization of silver nanoparticle-anchored amine-functionalized mesoporous silica for electrocatalytic determination of nitrite. J Solid State Electrochem. <https://doi.org/10.1007/s10008-014-2725-3>
- Sonkar PK, Ganesan V, Gupta R, Yadav DK (2016) Simple route to anchor silver nanoparticles into thiol-functionalized mesoporous silica: synthesis, characterization and electrochemical applications. J Nanoparticle Res. <https://doi.org/10.1007/s11051-016-3607-7>
- Suaarez MF, Mills A, Egdell RG, Compton RG (2000) Anodic stripping voltammetry with photochemical preconcentration at nanocrystalline TiO<sub>2</sub> films: detection of Ag and Hg<sup>2+</sup>. Electroanalysis. [https://doi.org/10.1002/\(SICI\)1521-4109\(20000401\)12:63.3.CO;2-9](https://doi.org/10.1002/(SICI)1521-4109(20000401)12:63.3.CO;2-9)
- Suherman AL, Ngamchuea K, Tanner EE, Sokolov SV, Holter J, Young NP, Compton RG (2017) Electrochemical detection of ultratrace (picomolar) levels of Hg<sup>2+</sup> using a silver nanoparticle-modified glassy carbon electrode. Anal Chem. <https://doi.org/10.1021/acs.analchem.7b01304>
- Tang Y, Allen BL, Kauffman DR, Star A (2009) Electrocatalytic activity of nitrogen-doped carbon nano tube cups. J Am Chem Soc. <https://doi.org/10.1021/ja904595t>
- Tang S, Tong P, Lu W, Chen J, Yan Z, Zhang L (2014) A novel label-free electrochemical sensor for Hg<sup>2+</sup> based on the catalytic formation of metal nanoparticle. Biosens Bioelectron. <https://doi.org/10.1016/j.bios.2014.02.074>
- Toh HS, Jurkschat K, Compton RG (2015) The influence of the capping agent on the oxidation of silver nanoparticles: nano-impacts versus stripping voltammetry. Chem Eur J 21:2998–3004. <https://doi.org/10.1002/chem.201406278>
- Tyagi CK, Jhade D, Shah SK (2016) Evaluation of anticoagulant activity of aqueous extract of *Cestrum nocturnum*. Int J Phytomed. <https://doi.org/10.5138/09750185.1969>
- Wang J, Bonakdar M (1988) Preconcentration and voltammetric measurement of mercury with a crown-ether modified-carbon-paste electrode. Talanta. [https://doi.org/10.1016/0039-9140\(88\)80085-7](https://doi.org/10.1016/0039-9140(88)80085-7)
- Wei Y, Yang R, Liu JH, Huang XJ (2013) Selective detection toward Hg (II) and Pb (II) using polypyrrole/carbonaceous nanospheres modified screen-printed electrode. Electrochim Acta. <https://doi.org/10.1016/j.electacta.2013.05.004>
- Wu L, Long Z, Liu L, Zhou Q, Lee YI, Zheng C (2012) Microwave-enhanced cold vapor generation for speciation analysis of mercury by atomic fluorescence spectrometry. Talanta. <https://doi.org/10.1016/j.talanta.2012.03.009>
- Zaib M, Athar MM, Saeed A, Farooq U (2015) Electrochemical determination of inorganic mercury and arsenic-a review. Biosens Bioelectron. <https://doi.org/10.1016/j.bios.2015.07.058>
- Zheng W, Aschner M, Ghersi-Egea JF (2003) Brain barrier systems: a new frontier in metal neurotoxicological research. Toxicol Appl Pharmacol. [https://doi.org/10.1016/S0041-008X\(03\)00251-5](https://doi.org/10.1016/S0041-008X(03)00251-5)
- Zhou N, Li J, Chen H, Liao C, Chen Z, Chen L (2013) A functional graphene oxide-ionic liquid composites/gold nanoparticles sensing platform for ultrasensitive electrochemical detection of Hg<sup>2+</sup>. Analyst. <https://doi.org/10.1039/C2AN36405K>

**Publisher's note** Springer Nature remains neutral with regard to jurisdictional claims in published maps and institutional affiliations.